Spin Density Distribution of α-Nitronyl Aminoxyl Radicals from Experimental and ab Initio Calculated ESR Isotropic Hyperfine Coupling Constants

Joan Cirujeda,[†] José Vidal-Gancedo,[†] Oriol Jürgens,[†] Fernando Mota,[‡] Juan J. Novoa,*[,‡] Concepció Rovira,[†] and Jaume Veciana*[,†]

Contribution from the Institut de Ciència de Materials de Barcelona (CSIC), Campus Universitari de Bellaterra, 08193 Cerdanyola, Spain, and Departament de Química Física and CER Química Teòrica, Universitat de Barcelona, Av. Diagonal 647, 08028 Barcelona, Spain

Received February 8, 2000. Revised Manuscript Received August 14, 2000

Abstract: Isotropic ESR spectra have been determined for the following α-nitronyl aminoxyl radicals showing different substituents at the 2-position of the imidazolyl ring: ^{1}H (**1**); ^{2}H (**2**); 3′,5′-(*t*-C_4H_9)$_2$-4′-(HO)C_6H_2 (**3**); 4′-HOC_6H_4 (**4**); 3′,5′-$(HO)_2C_6H_3$ (**5**); 3′-HOC_6H_4 (**6**); 3′,4′-$(HO)_2C_6H_3$ (**7**); C_6H_5 (**8**); 4′-$NO_2C_6H_4$ (**9**); 2′-HOC_6H_4 (**10**); 2′,4′-$(HO)_2C_6H_3$ (**11**); and 2′-ClC_6H_4 (**12**). Solvent dependence in a large variety of solvents of the isotropic ESR hyperfine coupling constants (hfcc's) for **1**, **4**, **6**, **8**, **9**, **10**, and **12** has been studied for the first time by the linear solvation energy relationship (LSER) methodology. From this study, the most important solvent−solute interactions governing the spin density distribution in these radicals as well as the estimates of their hyperfine coupling constants in the absence of any significant solvent−solute interaction have been determined. Such solvent-independent hyperfine coupling constants are the expected values in gas phase and, therefore, they are used to evaluate the theoretically calculated hfcc's, at the DFT/B3LYP/EPR-II level, to validate the level of precision of this theoretical method. It is found that ab initio calculations reproduce the order of magnitude and the trends of the solvent-independent hfcc's. Ab initio calculations also reproduce the main features of the atomic spin populations and the spin density maps experimentally found in the solid state by polarized neutron diffraction for radicals **8** and **9**.

Introduction

The design, preparation, and study of new, purely organic, magnetic materials, based on persistent α-nitronyl aminoxyl radicals,[1] has been the goal of many research groups during the past decade.[2] A complete understanding of magnetic phenomena shown by these materials requires an exact knowledge of the spin density distribution over the three-dimensional space surrounding the molecules used to construct the solids, since these spin distributions provide information about the mechanisms through which intermolecular magnetic interactions take place.[2] Until now, polarized neutron diffraction (PND) has proved to be the most powerful technique yielding detailed spin density distribution maps of several molecular magnetic materials,[3] including some based on α-nitronyl aminoxyl radicals.[4] The information in these maps is usually condensed under the form of atomic spin populations using various projection techniques. α-Nitronyl aminoxyl radicals show a large positive spin density on the four atoms of the two NO groups, a smaller negative spin density on the C atom joining them, and also null or vanishing spin densities, either positive or negative, on the remaining atoms of the molecule.[4] In cases which exhibit significant intermolecular magnetic interactions, this technique

* To whom correspondence should be addressed. Phone: +(34)-93-5801853. Fax: +(34)-93-5805729. E-mail: vecianaj@icmab.es. E-mail: novoa@qf.vb.es.

† Institut de Ciència de Materials de Barcelona.

‡ Universitat de Barcelona.

(1) α-Nitronyl aminoxyl radical is used throughout to indicate the correct IUPAC name: 4,5-dihydro-4,4,5,5-tetramethyl-3-oxido-1*H*-imidazol-3-ium-1-oxyl radical.

(2) For recent overviews on molecular magnetic materials, see: (a) Day, P., Underhill, A. E., Eds. Metal−organic and organic molecular metals. *Philos. Trans. R. Soc. London A* **1999**, *357*, 2851−3184. (b) Kahn, O., Ed. Proceedings of the 6th International Conference on Molecule Based Magnets. *Mol. Cryst. Liq. Cryst.* **1999**, *334*, 1−712; **1999**, *335*, 1−706. (c) *Magnetism: A Supramolecular Function*; Kahn, O., Ed.; Kluwer: Dordrecht, The Netherlands, 1996. (d) Kinoshita, M. *Jpn. J. Appl. Phys.* **1994**, *33*, 5718. (e) Miller, J. S.; Epstein, A. J. *Angew. Chem., Int. Ed. Engl.* **1994**, *33*, 385. (f) Kahn, O. *Molecular Magnetism*; VCH Publishers: New York, 1993.

(3) (a) Pontillon, Y. Ph.D. Thesis, Université Joseph Fourier-Grenoble I, France, 1997. (b) Zheludev, A.; Chiarelli, R.; Delley, B.; Gillon, B.; Rassat, A.; Ressouche, E.; Schweizer, J. *J. Magn. Magn. Mater.* **1995**, *140−144*, 1439−1440. (c) Zheludev, A. Ph.D. Thesis, Université Joseph Fourier-Grenoble I, France, 1994. (d) Zheludev, A.; Grand, A.; Ressouche, E.; Schweizer, J.; Morin, B. G.; Epstein, A. J.; Dixon, D. A.; Miller, J. S. *Angew. Chem., Int. Ed. Engl.* **1994**, *33*, 1397−1399. (e) Zheludev, A.; Grand, A.; Ressouche, E.; Schweizer, J.; Morin, B. G.; Epstein, A. J.; Dixon, D. A.; Miller, J. S. *J. Am. Chem. Soc.* **1994**, *116*, 7243−7249. (f) Figgis, B. N.; Kucharski, E. S.; Vrtis, M. *J. Am. Chem. Soc.* **1993**, *115*, 176−181. (g) Ressouche, E.; Boucherle, J. X.; Gillon, B.; Rey, P.; Schweizer *J. Am. Chem. Soc.* **1993**, *115*, 3610−3617 and references therein.

(4) (a) Schweitzer, J. *Physica B* **1997**, *234−236*, 772−779. (b) Pontillon, Y.; Ressouche, E.; Romero, F.; Schweitzer, J.; Ziessel, R. *Physica B* **1997**, *234−236*, 788−789. (c) Zhedulev, A.; Ressouche, Schweitzer, J.; Turek, P.; Wan, M.; Wang, H. *J. Magn. Magn. Mater.* **1995**, *140−141*, 1441−1442. (d) Zhedulev, A.; Barone, V.; Bonnet, M.; Delley, B.; Grand, A.; Ressouche, E.; Rey, P.; Subra, R.; Schweitzer, J. *J. Am. Chem. Soc.* **1994**, *116*, 2019−2027. (e) Ressouche, E.; Zheludev, A.; Boucherle, J. X.; Gillon, B.; Rey, P.; Schweizer, J. *Mol. Cryst. Liq. Cryst.* **1993**, *232*, 13−26. (f) Pontillon, Y.; Akita, T.; Grand, A.; Kobayashi, K.; Lelievre-Berna, E.; Pécaut, J.; Ressouche, E. Schweizer. *J. Am. Chem. Soc.* **1999**, *121*, 10126. (g) Pontillon, Y.; Caneschi, A.; Gatteschi, D.; Grand, A.; Ressouche, E.; Sessoli, R.; Schweizer, J. *Chem. Eur. J.* **1999**, *5*, 3616. (h) Heise, H.; Köhler, F. H.; Mota, F.; Novoa, J. J.; Veciana, J. *J. Am. Chem. Soc.* **1999**, *121*, 9659. (i) Romero, F. M.; Ziessel, R.; Bonnet, M.; Pontillon, Y.; Ressouche, E.; Schweizer, J.; Delley, B.; Grand, A.; Paulsen, C., *J. Am. Chem. Soc.* **2000**, *122*, 1298.

10.1021/ja0004884 CCC: $19.00
Published on Web 11/03/2000

also shows the presence of an abnormally large spin density on molecular regions close to the NO groups as a result of the spin polarization produced by the spins of neighboring molecules, revealing thus the importance of such regions for the magnetic coupling phenomenon.[5] Unfortunately, the high cost of PND experiments and the strict sample requirements—large single crystals—render the technique useless for routine characterization and does not permit a precise determination of the vanishing spin densities on some molecular regions which are at the limit of the experimental accuracy.[6] These regions are sometimes extremely important since they are the fingerprints of the presence of intermolecular magnetic interactions.[7] In fact, according to the most widely used structure−magnetism relationship, the McConnell I mechanism,[8] and recent studies on its scope and limitations,[9] both the nature and the strength of the magnetic exchange coupling between two neighboring molecules depend on the molecular spin density distribution as well as on the relative orientation of the two interacting molecules.

The accessible spectroscopic techniques, such as *e*lectron *s*pin *r*esonance (ESR),[10] *e*lectron *n*uclear *do*uble *r*esonance (ENDOR), and *n*uclear *m*agnetic *r*esonance (NMR),[11] yield direct experimental information about the electronic structure of open-shell molecules under a wide variety of experimental conditions. They all have different advantages and limitations that make them complementary to each other and also to PND measurements. In particular, ESR has proven to be a very powerful tool in assessing the electronic structure of purely organic radicals and transition metal complexes in frozen or fluid dilute solutions[12] and in the solid state,[13,14] providing different kinds of information. ESR measurements performed in dilute fluid solutions under high-resolution conditions provide extremely precise isotropic hyperfine coupling constants (hfcc's) for nuclei with both large and vanishing spin densities, unattainable with other techniques. Unfortunately, ESR spectroscopy does not provide the sign of the spin density—it gives only the absolute value—or the density on nuclei for isotopes having zero nuclear spin ($I = 0$). For these reasons, it is always convenient to combine these studies with another spectroscopic technique that furnishes these data, such as ^{1}H or ^{13}C NMR[12a,15] and ^{1}H ENDOR.[16] An alternative approach to the latter experimental techniques involves ab initio calculations using the adequate methodology, since they provide directly the strength and sign of the spin density on all nuclei, including those with zero nuclear spins. Previous computational studies on model radicals have shown that the B3LYP functional gives reasonable results for the spin distribution of these radicals, including a few small α-nitronyl aminoxyl radicals.[4,17]

As already mentioned, ESR of dilute fluid solutions under high-resolution conditions provides detailed data about the electronic structure of organic radicals. However, only very few studies of this kind have been performed to date,[12−16] and no such studies were performed systematically with the objective of mapping the spin density distribution of substituted α-nitronyl aminoxyl radicals. The aim of this work is to determine such spin density distributions as well as to evaluate how the substituents and the surrounding media—solvent molecules and neighboring radicals in the crystals—affect these spin distributions. We will do so by combining an ESR study in fluid solution with accurate ab initio computations, after calibrating the quality of these computations on this family of radicals, using different basis sets and methods which have previously been shown to give reasonable computed values of the spin distribution on model radicals.[4d,17] Our study will show that ab initio methods can be helpful to make proper assignments of complex ESR spectra and to determine the main features of the spin density distributions of this family of radicals.[4h]

The α-nitronyl aminoxyl radicals selected for this first systematic ESR study in fluid solution are the radicals **1**−**12** (Scheme 1).[18] The ESR study provides for each radical−solvent pair the values of the hfcc's which depend on the spin density on the nuclei and the nature of the solvent. To obtain solvent-independent hfcc's, we have carried out for the first time a *l*inear solvation *e*nergy *r*elationship[19] (LSER) analysis of liquid-state ESR data.[20] The hfcc's obtained from ab initio computations for all atoms of these radicals in a vacuum, using the B3LYP density functional and various basis sets, among them the EPR-II basis set, reproduce the trends observed for the extrapolated solvent-independent values. On the other hand, the computed spin density maps and atomic spin populations of two repre-

(5) See ref 4b.

(6) Atoms and substituents located at the periphery of the molecule, such as the methyl groups or phenyl substituents in α-nitronyl aminoxyl radicals, show very small spin densities that are not detectable by PND. These densities do, however, play a relevant role in the intermolecular magnetic interactions since they determine such magnetic interactions.

(7) (a) Matsushita, M.; Izuoka, A.; Sugawara, T.; Kobayashi, T.; Wada, N.; Takeda, N.; Ishikawa, M. *J. Am. Chem. Soc.* **1997**, *119*, 4369−4379. (b) Cirujeda, J.; Mas, M.; Molins, E.; Lanfranc de Panthou, F.; Laugier, J.; Park, J.; Paulsen, C.; Rey, P.; Rovira, C.; Veciana, J. *J. Chem. Soc., Chem. Commun.* **1995** 709−710.

(8) McConnell, H. R. *J. Chem. Phys.* **1963**, *39*, 1910.

(9) (a) Deumal, M.; Cirujeda, J.; Veciana, J.; Novoa, J. J. *Adv. Mater*. **1998**, *10*, 1461−1466. (b) Deumal, M.; Novoa, J. J.; Beapark, M.; Celani, P.; Olivucci, M.; Robb, M. A. *J. Phys. Chem. A* **1998**, *102*, 8404−8408. (c) Deumal, M.; Cirujeda, J.; Veciana, J.; Novoa, J. J. *Chem. Eur. J.* **1999**, *5*, 1631.

(10) (a) Weil, J. A.; Bolton, J. R.; Wertz, J. E. *Electron Paramagnetic Resonance*; John Wiley & Sons: New York, 1994. (b) Atherton, N. M. *Principles of Electron Spin Resonance*; Ellis Horwood Limited: London, 1993.

(11) (a) Yanoni, C. S. *Acc. Chem. Res.* **1982**, *15*, 201. (b) Voelkel, R *Angew. Chem., Int. Ed. Engl.* **1988**, *27*, 1468. (c) Ferrieu, F.; Nechstein, M. *Chem. Phys. Lett.* **1971**, *11*, 46−50. (d) Ondercin, D.; Sandreczki, T.; Kreilick, R. W. *J. Magn. Reson*. **1979**, *34*, 151−159. (e) Hentsch, F.; Helmle, M.; Köngeter, D.; Mehring, M. *Ber. Bunsen-Ges. Phys. Chem*. **1987**, *91*, 911−913. (f) Groombridge, C. J.; Perkins, M. J. *J. Chem. Soc., Chem. Commun*. **1991**, 1164−1166. (g) Barrie, P. J.; Groombridge, C. J.; Grossel, M. C.; Weston, S. C. *J. Chem. Soc*., *Chem. Commun*. **1992**, 1216−1218. (h) Chen, J.; Cai, F.-F.; Shao, Q.-F.; Huang, Z.-E.; Chen, S.-M. *J. Chem. Soc., Chem. Commun*. **1996**, 1111−1112.

(12) (a) Kreilick, R. W.; Becher, J.; Ullman, E. F. *J. Am. Chem. Soc*. **1969**, *91*, 5121−5124. (b) D'Anna, J. A.; Wharton, J. H. *J. Chem. Phys*. **1970**, *53*, 4047−4052. (c) Ullman, E. F.; Osiecki, J. H.; Boocock, D. G. B., Darcy, R. *J. Chem. Phys.* **1972**, *94*, 7049−7059. (d) Goldman, J.; Petersen, T. E.; Torssell, K.; Becher, J. *Tetrahedron* **1973**, *29*, 3833−3843.

(13) Bencini, A.; Gatteschi, D. *EPR of Exchange Coupled Systems*; Springer-Verlag: New York, 1990.

(14) (a) Tamura, M.; Nakazawa, Y.; Shiomi, D.; Nozawa, K.; Hosokoshi, Y.; Ishikawa, M.; Takahashi, M.; Kinoshita, M. *Chem. Phys. Lett*. **1991**, *186*, 401. (b) Nakazawa, Y.; Tamura, M.; Shirakawa, M.; Shiomi, D.; Takahashi, M.; Kinoshita, M.; Ishikawa, M. *Phys. Rev. B* **1992**, *46*, 8906−8908. (c) Cirujeda, J.; Hernàndez-Gasio, E.; Rovira, C.; Stanger, J.-L.; Turek, Ph. *J. Mater. Chem.* **1995**, *5*, 243−252.

(15) (a) Davis, M. S.; Morokuma, K.; Kreilick, R. W. *J. Am. Chem. Soc*. **1972**, *94*, 5588−5592. (b) Neely, J. W.; Hatch, G. F.; Kreilick, R. W. *J. Am. Chem. Soc*. **1974**, *96*, 652−656.

(16) (a) Ottaviani, M. F. *J. Chem. Soc., Faraday Trans.* **1990**, *86*, 3211−3219. (b) Takui, T.; Miura, Y.; Inui, K.; Teki, Y.; Inoue, M.; Itoh, K. *Mol. Cryst. Liq. Cryst*. **1995**, *271*, 55−66.

(17) (a) Barone, V.; Bencini, A.; di Natteo, A. *J. Am. Chem. Soc*. **1997**, *119*, 10831. (b) Novoa, J. J.; Mota, F.; Veciana, J.; Cirujeda, J. *Mol. Cryst. Liq. Cryst.* **1995**, *271*, 79−90.

(18) A complementary study, both in solid and in solution, of this family of radicals but using ^{1}H and ^{13}C NMR has been recently performed. See ref 4h.

(19) (a) Abboud, J.-L. M.; Kamlet, M. J.; Taft, R. W. *J. Am. Chem. Soc.* **1977**, *99* 6027. (b) Reichart, C. *Solvent and Solvent Effects in Organic Chemistry*; VCH: New York, 1990.

(20) Up to now and to our knowledge this method has not been applied for any α-nitronyl aminoxyl radical. Only some aminoxyl radicals have been studied by LSER. See: Knauer, B. R.; Napier, J. J. *J. Am. Chem. Soc*. **1976**, *98*, 4395−4400.

Scheme 1

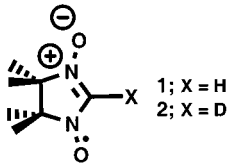

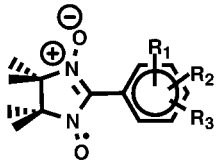

3; R_1 = 3-*tert*Bu, R_2 = 4-OH, R_3 = 5-*tert*Bu
4; $R_1 = R_2$ = H, R_3 = 4-OH
5; R_1 = H, R_2 = 3-OH, R_3 = 5-OH
6; $R_1 = R_2$ = H, R_3 = 3-OH
7; R_1 = H, R_2 = 3-OH, R_3 = 4-OH
8; $R_1 = R_2 = R_3$ = H
9; $R_1 = R_2$ = H, R_3 = 4-NO_2
10; $R_1 = R_2$ = H, R_3 = 2-OH
11; R_1 =H, R_2 = 2-OH, R_3 = 4-OH
12; R_1 = H, R_2 = 2-Cl, R_3 = 4-OH

sentative radicals reproduce the main features obtained from PND experiments with solid samples. Therefore, this computational methodology is a useful tool to gain information on the basic principles of the magnetic interactions that these radicals can undergo in molecular crystals.

Experimental Section

Materials. Reagents and solvents for synthesis of radicals were purchased from Aldrich and purified according to accepted procedures.[21] Substituted α-nitronyl aminoxyl radicals **1**−**12** were synthesized by following the Ullman's procedure as previously reported.[22] Solvents used for the ESR study were all of spectrograde quality (Romil, Fluka, and SDS) and were used fresh as received.

Measurements. X-band (9.5 GHz) ESR spectra were recorded on a standard Bruker continuous-wave spectrometer of the ESP-300E series, equipped with a field−frequency (F/F) lock accessory and a built-in NMR Gaussmeter. A rectangular TE102 cavity was used for the measurements. The spectrometer was also equipped with a Bruker ER 4121 HT nitrogen cryostat controlled by an Oxford ITC4 temperature control unit. The signal-to-noise ratio of the spectra was increased by accumulation of scans using the F/F lock accessory in order to guarantee large field reproducibility in each scan. Precautions to avoid undesirable spectral distortions and line broadenings, such as those arising from microwave power saturation and magnetic field overmodulation, were also taken into account. To avoid dipolar line broadening (from dissolved O_2), solutions were always carefully degassed three times using vacuum−thaw cycles with pure Ar. High-resolution isotropic ESR spectra were obtained by an optimal choice of the experimental conditions—temperature, viscosity, and radical concentration—that reduce the spectral line width to the minimum. The optimal experimental conditions were found to be similar for all studied radicals: moderate viscosities, $\eta \geq 25$ cP, intermediate temperatures, $220 \leq T \leq 300$ K, and low radical concentrations, $c \leq 5 \times 10^{-5}$ M. Under these conditions, the lowest intrinsic line width achieved was 70 mG. The nature of the solvent also influences notably the signal line width because the solvent modifies rates (through changes in the viscosity and in the molecular solvation), the effective collision cross section of these radical molecules, and their tumbling. The use of experimental conditions different from the optimal ones leads to low-resolution isotropic ESR spectra in which severe overlapping of lines is produced. Computer simulations of experimental isotropic spectra were carried out with the EPRFTSM program.[23] Due to the low natural isotopic abundance of ^{13}C atoms in the studied radicals, it was only possible to observe the largest hyperfine coupling constants with such nuclei, i.e., those of the α-carbon atom. This coupling appears in the ESR spectrum as low-intensity satellite lines. Isotropic ESR spectra of studied radicals were recorded in 26 different solvents, representative of the most important solute−solvent interactions.[24] Solvents employed were the following: *n*-pentane, *n*-hexane, toluene, chlorobenzene, carbon disulfide, carbon tetrachloride, chloroform, dichloromethane, diisopropyl ether, diethyl ether, tetrahydrofuran, *p*-dioxan, acetone, acetonitrile, ethyl acetate, nitromethane, nitrobenzene, pyridine, triethylamine, dimethylformamide, dimethyl sulfoxide, ethanol, methanol, benzyl alcohol, water, and acetic acid. Multivariable linear regressions of the hfcc's obtained by simulation of the high-resolution experimental spectra in the 26 studied solvents were performed using the SYSTAT program.[25]

Computational Details. The isotropic hyperfine coupling constant of a nucleus X, $a(X)$, can be computed from the nuclear spin density, $\rho(r_X)$, using the following equation,

$$a(X) = 8\pi/3(g_e/g_0)\gamma_X\beta_X\rho(r_X) \quad (1)$$

where g_0 is the isotropic *g*-value for the radical, g_e the *g*-value for the free electron, γ_X the gyromagnetic nuclear ratio, and β_X the nuclear magneton of the nucleus X. The spin density on each nucleus is calculated with the GAUSSIAN-94 suite of programs (Fermi contact terms), using the spin density function.

Ab initio computation of hfcc's has been carried out previously on many open-shell systems, among others on the first-row atoms[26] and their hydrides,[27] the hydroxyl radical and five peroxyl radicals,[28] a subset of π-radicals,[29] and various NO-containing radicals which included the radical **1**.[30] Also interesting are those studies covering a wide variety of radicals, like those of Eriksson et al.,[31] Wang et al.,[32] or Gauld et al.[33] The overall picture emerging from all of these previous studies is the dependence of the computed hfcc's on the method and the basis set selected: good results are generally found using the QCISD method or the B3LYP density functional and basis set, which describe well the core region of the electron density, like the IGLO-III,[34] the EPR-II and EPR-III basis of Barone,[35] the core-valence correlation-consistent cc-pCVXZ,[36] and the s-uncontracted cc-uspVXZ basis sets.[37] Even with these basis sets and the QCISD method, the mean absolute deviation from the experimental values in a subset of di-, tri-, and tetraradicals can be as large as 4.5 G, and a similar value is obtained using the B3LYP functional.[33] Interestingly, the hfcc's computed for these radicals

(21) Gordon, A. J.; Ford, R. A. *The Chemist's Companion*; John Wiley & Sons: New York, 1972.
(22) Ullman, E. F.; Osiecki, J. H.; Boocock, D. G. B.; Darcy, R. *J. Am. Chem. Soc.* **1972**, *94*, 7049 and references therein.
(23) Kirste, B., EPRFTSM Program, Freie Universität Berlin, 1991.
(24) Ventosa, N.; Ruiz-Molina, D.; Sedó, J.; Rovira, C.; Tomas, X.; André, J.-J.; Bieber, A.; Veciana, J. *Chem. Eur. J.* **1999**, *5*, 3533.
(25) SYSTAT (5.01) Program; Systat Inc., Evanston, IL, 1994.
(26) (a) Carmichael, I. J. *Phys. Chem. A* **1997**, 1010, 4633. (b) Barone, V. *Chem. Phys. Lett.* **1994**, *226*, 392.
(27) Chipman, D. M. J. *Chem. Phys.* **1989**, *91*, 5455.
(28) Wetmore, S. D.; Boyd, R. J.; Eriksson, L. A. *J. Chem. Phys.* **1997**, *106*, 7738. Wetmore, S. D.; Eriksson, L. A.; Boyd, R. J. *J. Chem. Phys.* **1998**, *109*, 9451.
(29) Adamo, C.; Barone, V.; Fortunelli, A. *J. Chem. Phys.* **1995**, *102*, 384.
(30) (a) Adamo, C.; di Matteo, A.; Rey, P.; Barone, V. *J. Phys. Chem. A* **1999**, *103*, 3481. (b) Barone, V.; Bencini, A.; Cossi, M.; di Matteo, A.; Mattesini, M.; Totti, F. *J. Am. Chem. Soc.* **1998**, *120*, 7069.
(31) Eriksson, L. A.; Malkin, V. G.; Malkina, O. I.; Salahub, D. R. *J. Chem. Phys.* **1963**, *99*, 9756. Eriksson, L. A.; Malkin, V. G.; Malkina, O. I.; Salahub, D. R. *Int. J. Quantum Chem.* **1994**, *52*, 879.
(32) Wang, J.; Johnson, B. G.; Boyd, R. J.; Eriksson, L. A. *J. Phys. Chem.* **1996**, *100*, 6317.
(33) Gauld, J. W.; Eriksson, L. A.; Radom, L. *J. Phys. Chem. A* **1997**, *101*, 1352.
(34) Kutzelnigg, W.; Fleischer, U.; Schindler, M. *NMR—Basic Principles and Progress*; Springer: Heidelberg, 1990; Vol. 23, p 165.
(35) Barone, V. *Recent Advances in Density Functional Theory*, Part 1; Cong, D. P., Ed.; World Scientific Publishing Co.: Singapore, 1995; p 287.
(36) Woon, D. E.; Dunning, T. H. *J. Chem. Phys.* **1995**, *103*, 4572.
(37) Obtained by fully decontracting the inner *s* component of the cc-pVXZ basis sets.

Table 1. Isotropic hfcc's (in Gauss) Computed for the First Row Atoms with the Indicated Basis Sets and Using the B3LYP Functional and the UHF Method

basis set	B	C	N	O	F
IGLO-III	7.1	9.2	3.6	−9.3	72.9
EPR-II	3.9	7.7	2.9	−6.9	49.1
EPR-III	6.2	8.2	3.5	−9.0	74.9
cc-pCVDZ	2.3	0.1	−1.1	5.5	−74.2
cc-pCVTZ	3.5	5.8	2.5	−7.5	61.7
aug-cc-pCVDZ	4.3	3.0	0.2	2.2	−46.0
aug-cc-pCVTZ	4.6	7.5	3.2	−9.3	77.4
cc-uspVDZ	6.1	7.4	2.7	−6.6	48.6
cc-uspVTZ	6.0	7.9	3.1	−7.9	62.9
aug- cc-uspVDZ	8.0	10.4	4.0	−9.8	76.8
aug- cc-uspVTZ	8.2	10.4	4.0	−9.9	77.3
exptl hfcc	*4.1*	*7.0*	*3.7*	*−12.3*	*107.8*

at the QCISD/6-311+G(2df,p) level are better than those obtained at the QCISD/IGLO-III level, while the two basis perform equally well at the B3LYP level.[33] However, one has to keep in mind here that part of the success of the B3LYP method has been attributed to a fortuitous cancellation of errors, at least in some systems.[26] This fact explains that higher quality basis sets do not always provide hfcc values closer to the experimental results, as is found with the QCISD values. This failure is clearly illustrated in Table 1, which collects the B3LYP hfcc's computed for the first-row atoms with some of the basis sets which were identified in the literature as capable of providing accurate hfcc results at the QCISD level.[26−33]

The use of computed hfcc's to complement the extrapolated solvent-independent ESR values for of α-nitronyl aminoxyl radicals seems very attractive. However, despite the importance of these radicals in the field of molecular magnetism,[38] only a few ab initio methods have been aimed at computing their hfcc's: some focused on simple models of these radicals,[30b−39] and only five recent studies were focused on large α-nitronyl aminoxyl radicals.[4d−g,30a] These studies showed a fair agreement between the experimental hfcc's and the values computed at the B3LYP/EPR-II level, involving the underestimation of the *N* values in the 1.8−2.2 G range. However, there is no systematic study on a large series of α-nitronyl aminoxyl radicals using a methodology tested to give accurate results for these radicals. Previous work seems to indicate that the B3LYP nonlocal exchange and correlation functional gives reasonable results in many cases. However, after considering the results of Table 1, we decided to evaluate the quality of the hfcc's provided by various basis sets against the *solvent-independent data* obtained here for radical **1**, the simplest member of the α-nitronyl aminoxyl radicals. This is important since most of the comparisons carried out previously have been done on solvent-dependent data, and this can give rise to the wrong conclusions, given the non-negligible effect (vide infra) of the solvent on the measured hfcc's.

Results and Discussion

Experimental Isotropic ESR Spectra. ESR spectra of dilute fluid solutions of radicals **1**−**12** in all studied solvents consist of five equally spaced groups of signals with intensity ratios of 1:2:3:2:1, due to the coupling of the unpaired electron with two equivalent N nuclei. Each of these groups of signals is composed of a large number of lines due to further couplings with all the magnetically active nuclei (H, N, Cl, etc.) of the radicals. Such lines appear either completely or partially resolved, depending on the nature of substituents at the α C atom and on the experimental conditions in which the spectra were recorded (temperature, radical concentration, viscosity, and solvent nature). Most of these hyperfine couplings can be resolved when operating at high-resolution conditions. These conditions were achieved by decreasing to the maximum possible level the molecular collisions occurring in the fluid solutions (low temperatures, high viscosities, and low solvation conditions) and by increasing at the same time, as much as possible, the molecular tumbling rates (high temperatures and low viscosities). These conditions minimize the efficiency of the spin−spin relaxation mechanism and maximize the averaging of the magnetic anisotropy, leading to a decrease of the line widths.[10]

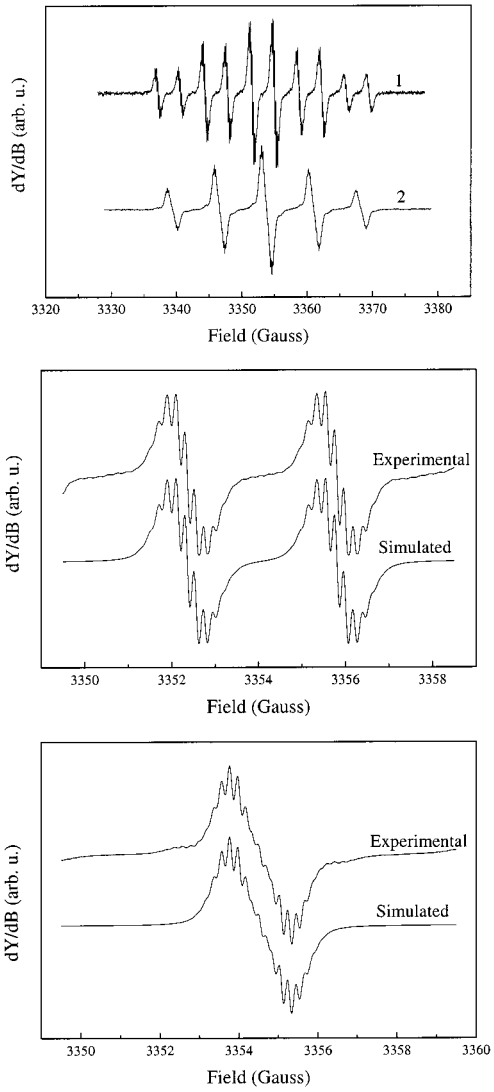

Figure 1. Experimental ESR spectra of radicals **1** and **2** under high-resolution conditions (top). Experimental and simulated central group of lines of radical **1** (middle) and radical **2** (bottom).

Figure 1 shows the spectra of radicals **1** and **2** in CCl_4 at 300 K, obtained under high-resolution conditions, together with the simulation of their central groups of lines. These simulations required the introduction of hyperfine couplings with 2 equivalent N nuclei and 12 equivalent H nuclei, along with an additional ^1H (or ^2H) nucleus for radical **1** (or **2**).[40] Values for the isotropic hfcc's found for both radicals by simulation are given in Table 2.

Simulation of the high-resolution spectra of **3**−**12** in CCl_4 at 300 K also revealed couplings with 2 N nuclei and 12 equivalent

(38) Tamaura, M.; Nakazawa, Y.; Shiomi, D.; Nozawa, K.; Hosokoshi, Y.; Ishikawa, M.; Takahashi, M.; Kinoshita, M. *Chem. Phys. Lett.* **1991**, *186*, 401.

(39) (a) Barone, V.; Lelj, F. N.; Russo, N.; Ellinger, Y.; Subra, R. *Chem. Phys.* **1983**, *76*, 385. (b) Grand, A.; Rey, P.; Subra, R.; Barone, V.; Minichino, C. *J. Phys. Chem.* **1991**, *95*, 9238.

(40) As theoretically expected, the ratio of the hfcc values found by simulation for the ^1H and ^2H atoms at the α-positions for radicals **1** and **2**, $|a_H|/|a_D| = 6.55$, is identical with the ratio of gyromagnetic constants for these two isotopes; $\gamma_H/\gamma_D = 6.51$. See eq 1 and ref 10.

Table 2. Isotropic Hyperfine Coupling Constants (in Gauss) and Linewidths (in Gauss) Used in the Simulation of Experimental ESR Spectra of Radicals **1**−**12** in CCl_4 at 300 K

radical	$\Delta B_{1/2}$	$\lvert a(\mathrm{N})\rvert$	$\lvert a(\mathrm{H_{CH_3}})\rvert$	$\lvert a(\mathrm{H_{ortho}})\rvert$	$\lvert a(\mathrm{H_{meta}})\rvert$	$\lvert a(\mathrm{H_{para}})\rvert$	$\lvert a(\mathrm{X})\rvert$	$\lvert a(^{13}C_\alpha)\rvert$
1	0.1856(4)	7.2190(2)	0.2026(2)				3.4472(6)[a]	*e*
2	0.1892(7)	7.2220(8)	0.2038(3)				0.5258(4)[b]	12.3
3	0.0883(3)	7.5668(5)	0.2121(1)	0.5151(3)				12.13
4	0.1409(7)	7.5066(5)	0.2072(3)	0.4985(2)	0.177(1)			12.5
5	0.1190(4)	7.6450(5)	0.2047(4)	0.4694(3)		0.392(2)		*e*
6	0.1316(8)	7.4453(4)	0.2100(6)	0.4986(5) 0.5193(4)	0.187(3)	0.421(3)		*e*
7	0.1086(4)	7.5274(6)	0.2100(1)	0.4793(2) 0.5496(1)	0.172(1)			*e*
8	0.1007(7)	7.4352(4)	0.2091(4)	0.4948(2)	0.1730(6)	0.421(2)		12.0
9	0.0995(8)	7.3605(8)	0.2037(6)	0.5210(3)	0.197(3)		0.103(1)[c]	11.8
10	0.123(2)	7.330(3) 7.814(3)	0.191(2)	0.347(9)	0.149(8)	0.304(1)		*e*
11	0.139(3)	7.216(5) 7.998(5)	0.182(6)	0.310(2)	0.140(20)			*e*
12	0.120(4)	7.3507(7)	0.199(1)	0.225(3)	0.160(6)		0.080(5)[d]	*e*

[a] hfcc with the ^{1}H nucleus at the α position. [b] hfcc with the ^{2}H nucleus at the α position. [c] hfcc with the N nucleus of NO_2 group at the para position. [d] hfcc with a ^{35}Cl nucleus at the ortho position, assuming that only this isotope is present. [e] Not observed due to unfavorable line widths.

Table 3. Normalized Regression Coefficients (*a*, *b*, *s*, *d*) and Solvent-Independent Values, $\lvert a(\mathrm{X})\rvert_0$ (in Gauss) Obtained by LSER Analyses of the Experimental Hyperfine Coupling Constants of Radicals **1**, **4**, **6**, **8**, **9**, **10**, and **12**, Obtained in 26 Different Solvents

radical	nucleus	$\lvert a(\mathrm{X})\rvert_0$	*a*	*b*	*s*	*d*	r^2
1	N	7.141 (23)	0.649 (47)	−0.092 (50)	0.608 (53)	−0.196 (52)	0.964
4	N	7.449 (11)	0.694 (41)	−0.033 (45)	0.627 (45)	−0.217 (45)	0.976
6	N	7.392 (16)	0.716 (59)	−0.092 (65)	0.612 (68)	−0.154 (68)	0.943
8	N	7.366 (12)	0.688 (43)	−0.109 (48)	0.677 (49)	−0.195 (50)	0.970
9	N	7.290 (14)	0.560 (56)	−0.147 (62)	0.812 (64)	−0.298 (65)	0.949
10[a]	N	7.501 (12)	0.473 (62)	−0.203 (64)	0.894 (67)	−0.388 (70)	0.947
12	N	7.248 (19)	0.788 (56)	−0.181 (64)	0.558 (65)	−0.188 (66)	0.945
1	H_α	3.500(13)	−0.66(10)		−0.43(10)	−0.14(10)	0.827
4	H_{ortho}	0.504(7)	−0.762(68)		−0.410(69)	0.099(69)	0.927
6	H_{ortho}	0.533(9)	−0.72(7)		−0.47(7)	0.16(7)	0.929
8	H_{ortho}	0.507(14)	−0.72(11)		−0.42(11)	0.05(11)	0.812
9	H_{ortho}	0.604(39)	−0.56(15)		−0.47(14)	0.21(15)	0.689
10	H_{ortho}	0.395(40)	−0.32(21)		−0.51(21)	0.31(22)	0.794
6	H_{para}	0.488(13)	−0.654(12)		−0.428(12)	0.12(10)	0.764
8	H_{para}	0.477(18)	−0.62(13)		−0.51(12)	0.05(12)	0.768
10	H_{para}	0.490(15)	−0.60(19)		−0.59(13)	0.06(13)	0.781
4−**12**	H_{meta}[b]	0.187(10)					
1−**12**	H_{methyl}[b]	0.213(10)					

[a] The mean value of the two $\lvert a(\mathrm{N})\rvert$ values observed in apolar solvents was used for the LSER analysis. [b] No solvent dependence has been found.

H nuclei, along with another magnetically active nucleus (Table 3). Figure 2 shows, as a representative example, the experimental and simulated spectra obtained under high-resolution conditions for radical **3**. The existence of a set of 12 equivalent H atoms in all studied radicals indicates that the equatorial and axial CH_3 groups of the five-membered rings are rapidly exchanging, through an inversion of the conformation—twisted and envelope—of the five-membered ring,[41,42] and also that these groups are rapidly rotating around the C−C σ bonds. Therefore, both motional processes must have rates faster than the ESR time scale (i.e., rates $>10^{10}$ s^{-1}). On the other hand, the equivalence of the two N nuclei observed for radicals **3**−**5** and **8** and **9** and in particular for radicals **6**, **7**, and **12** with phenyl rings lacking local C_2 symmetry suggests that these rings are rapidly oscillating between two potential energy wells or may be freely rotating on the ESR time scale with respect to the five-membered ring. It is also worth noting here the nonequivalence of the two N atoms observed for radicals **10** and **11**, both having one OH group at the ortho position, in their high-resolution spectra in CCl_4 at 300 K. Such nonequivalency is lost if any polar solvent (protic or aprotic) is added to the CCl_4 solution, thus indicating the establishment of a strong intramolecular hydrogen bond in this apolar solvent between the neighboring OH and NO groups that precludes the movement of phenyl rings.[43]

The comparison of the hfcc values for the aromatic H nuclei for radicals **3**−**9**, having similar steric constraints between the two rings (i.e., without substituents at the ortho positions) but with different substitution patterns, allowed an unambiguous assignment of all of the hfcc's. The resulting assignments for radical **8** (Table 2) are in full agreement with those previously obtained by other authors using ^{1}H NMR and ENDOR spectroscopies.[12−15] For radicals **2**, **3**, **4**, **8**, and **9**, which show favorable line widths and line shapes, it was also possible to observe the hyperfine coupling of the unpaired electron with

(41) (a) Cremer, D.; Pople, J. A. *J. Am. Chem. Soc.* **1975**, *97*, 1354. Dunitz, J. D. *Tetrahedron* **1972**, *28*, 5459. (b) Altona, C.; Sundaralingam, M. *J. Am. Chem. Soc.* **1972**, *94*, 8205. (c) Lowe, A. *Prog. Phys. Org. Chem.* **1968**, *6*, 1.

(42) (a) Amabilino, D. B.; Cirujeda, J.; Veciana, J. *Philos. Trans. R. Soc. London A* **1999**, *357*, 2873. (b) Minguet, M.; Amabilino, D. B.; Cirujeda, J.; Wurst, K.; Mata, I.; Molins, E.; Novoa, J. J.; Veciana, J. *Chem. Eur. J.* **2000**, *6*, 2350.

(43) Unfortunately, we were not able to observe any coupling with the H nucleus of the OH group, nor any significant change in the spectrum of the deuterated radical **10**, because the corresponding lines remain completely unresolved due to the small value of the corresponding hfcc. See ref 4h for experimental evidence about this point.

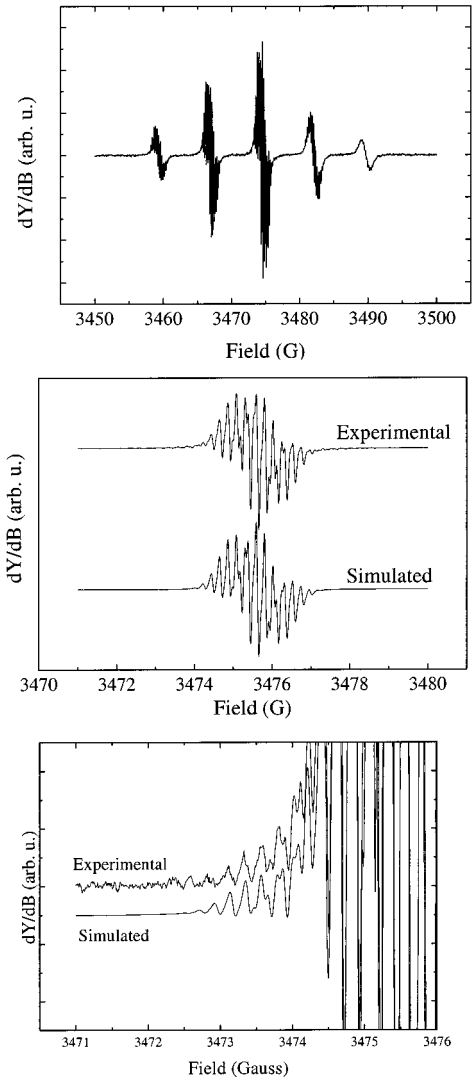

Figure 2. Experimental ESR spectra of radical **3** under high-resolution conditions (top). Experimental and simulated central group of lines of radical **3** (middle). Experimental and simulated satellite lines of radical **3** (bottom) due to the coupling with the α ^{13}C nucleus.

the natural ^{13}C isotope ($I = {}^1/_2$, 1.1% of abundance) at the α position that shows a mean value of 12.1 ± 0.2 G. This coupling is responsible for the weak satellite lines appearing beside each group of main signals (Figure 2).

It is important to stress the similarity of the aromatic hfcc's found for radicals with similar steric constrains between the two rings; i.e., radicals **3**−**9**. *This fact indicates that the spin density distributions on the phenyl rings are not strongly dependent on the nature and positions of the substituents on the aromatic ring*. The small, but significant, changes on the hfcc's observed for radicals that have substituents at the ortho positions (radicals **10**−**12**, see Table 2) can therefore be attributed to the modification of the relative conformation of the two rings. These changes could be produced either by the bulky atoms (Cl) or by the presence of substituents able to make intramolecular H bonds with the nearby NO groups. Another factor that modifies the spin density distribution of this family of radicals is the surrounding solvent medium. Thus, for a given radical the change of the solvent produces variations of $|a(\mathrm{N})|$ and $|a(\mathrm{H})|$ values up to 20% and 30%, respectively. In an effort to ascertain the origins of such changes, we used an LSER analysis[44−47] of the hfcc's for the representative radicals **1**, **4**, **6**, **8**, **9**, **10**, and **12**. Treatment of the hfcc values with the multiparametric eq 2, developed by Kamlet, Taft, et al.,[19] revealed the most important physicochemical properties of the employed solvents that influence the spin density distribution of these radicals. This equation describes the solvent effects on

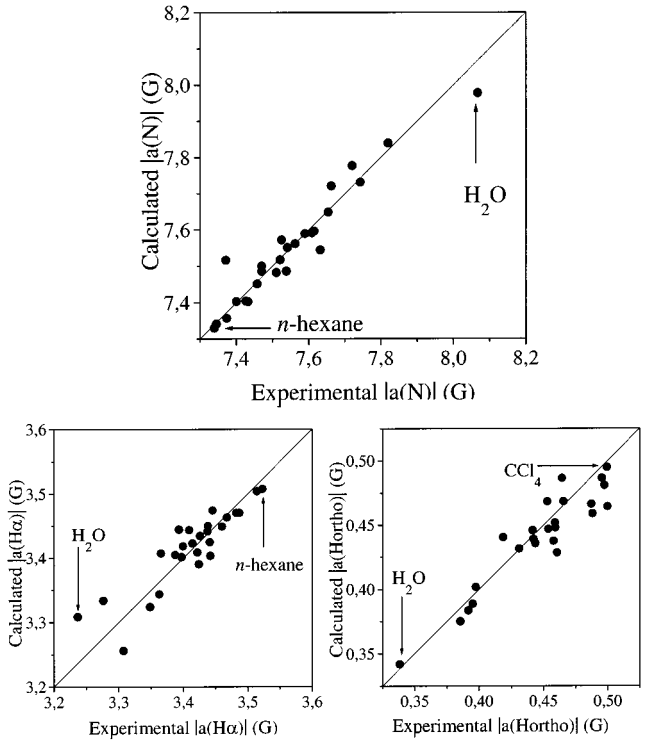

Figure 3. Multivariable correlations with eq 2 in 26 different solvents for $|a(\mathrm{N})|$ values of radical **8** (top), $|a(\mathrm{H})|$ values of the α H atom of radical **1** (bottom, left), and $|a(\mathrm{H})|$ values of the ortho H atoms of radical **8** (bottom, right).

Scheme 2

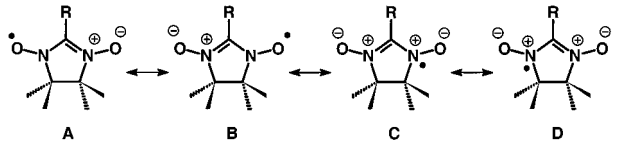

$$|a(\mathrm{X})| = |a(\mathrm{X})|_0 + a\alpha + b\beta + s(\pi^* + d\delta) + c\Omega + e\xi \quad (2)$$

an observable of the solute—in this case the hfcc with the nuclei X of a given radical, $|a(\mathrm{X})|$—as a linear combination of different parameters characterizing the solvent (α, β, π^*, δ, Ω, and ξ), weighted by factors (*a*, *b*, *s*, *d*, *c*, and *e*) which determine the importance of each solute−solvent interaction for the observable. In eq 2, $|a(\mathrm{X})|_0$ is the hfcc in the absence of any solute−solvent interaction and represents the expected value of $|a(\mathrm{X})|$ for isolated molecules, an estimate of the *gas-phase* value. The α parameter[44] reflects the hydrogen bond donor acidity of the solvent, and the β parameter[45] provides a measure of the solvent's hydrogen bond acceptor ability, while the π^* parameter[46] is an index of solvent polarity/polarizability, and the δ parameter[47] is a correction term of the polarizability for

(44) Taft, R. W.; Kamlet, M. J. *J. Am. Chem. Soc.* **1976**, *98*, 2886.
(45) Taft, R. W.; Kamlet, M. J. *J. Am. Chem. Soc.* **1976**, *98*, 377.
(46) (a) Taft, R. W.; Kamlet, M. J.; Abboud, J.-L. M., *J. Am. Chem. Soc.* **1977**, *98*, 6027. (b) Taft, R. W.; Kamlet, M. J., *J. Chem. Soc., Perkin. Trans. 2* **1979**, 349−356.
(47) Taft, R. W.; Abboud, J.-L. M.; Kamlet, M. J. *J. Am. Chem. Soc.* **1981**, *103*, 1080−1086.

Table 4. Calculated B3LYP Isotropic Hyperfine Coupling Constants (in Gauss) for the Optimized Geometry of Radical **1** Using Various Basis Sets[a]

		basis set					
atom	EPR-II	cc-pVDZ	cc-pVTZ	cc-pCVDZ	cc-pCVTZ	cc-uspVDZ	cc-uspVTZ
H1	5.96	5.25	5.46	5.21	5.42	4.95	5.38
C2	−15.05	−17.06	−10.44	−12.75	−13.75	−14.50	−14.40
N3	5.15	6.94	3.24	3.62	5.10	4.88	5.25
N4	5.15	6.94	3.24	3.62	5.10	4.88	5.25
O5	−9.49	−16.63	−6.04	−4.78	−9.96	−9.14	−9.96
O6	−9.49	−16.63	−6.04	−4.78	−9.96	−9.14	−9.96
C7	−2.65	−2.80	−2.22	−2.50	−2.46	−2.60	−2.52
C8	−2.65	−2.80	−2.22	−2.50	−2.46	−2.60	−2.52
C9	3.53	3.26	3.18	3.10	3.32	3.19	3.31
C10	1.56	1.71	1.56	1.52	1.60	1.55	1.58
C17	3.53	3.26	3.18	3.10	3.32	3.19	3.31
C18	1.56	1.71	1.56	1.52	1.60	1.55	1.58
H11	−0.24	−0.21	−0.22	−0.20	−0.21	−0.21	−0.21
H12	−0.32	−0.28	−0.31	−0.28	−0.32	−0.28	−0.32
H13	−0.25	−0.23	−0.21	−0.22	−0.22	−0.21	−0.22
H14	0.42	0.32	0.44	0.32	0.42	0.35	0.41
H15	−0.67	−0.54	−0.62	−0.55	−0.63	−0.56	−0.62
H16	−0.38	−0.31	−0.33	−0.31	−0.33	−0.30	−0.34
H19	−0.32	−0.28	−0.31	−0.28	−0.32	−0.28	−0.32
H20	−0.25	−0.23	−0.21	−0.22	−0.22	−0.21	−0.22
H21	−0.24	−0.21	−0.22	−0.20	−0.21	−0.21	−0.21
H22	−0.38	−0.31	−0.33	−0.31	−0.33	−0.30	−0.34
H23	0.42	0.32	0.44	0.32	0.42	0.35	0.41
H24	−0.67	−0.54	−0.62	−0.55	−0.63	−0.56	−0.62
n	143	119	512	133	655	161	604

[a] The full geometry optimization was carried out at the B3LYP/aug-cc-pVDZ level, giving rise to a geometry very similar to that observed in the solid state. The size of each basis set (*n*) is also indicated.

polychlorinated and aromatic solvents. The Ω parameter, also named the cavity term or cavitational parameter,[48] is a measure of the solvent/solvent interactions that are destroyed in creating the cavity for locating the solute molecules. Finally, the ξ parameter has been useful in correlating certain types of basicity properties of solvents.[49] Figure 3 shows some of the multivariable correlations achieved with eq 2 for selected hfcc's of radicals **1** and **8**.

The results of the LSER analysis for the $|a(\mathrm{N})|$ and various $|a(\mathrm{H})|$ constants of all the studied radicals are collected in Table 3. Nuclei not included in Table 3 either give very poor regression coefficients in the LSER analysis or are magnetically silent in the ESR spectra. Concerning the $|a(\mathrm{N})|$ values, the dominant parameters are the hydrogen bond donor acidity (α) and the polarity/polarizability (π^* and δ) of the solvent, both having significant positive influence. The hydrogen bond acceptor basicity (β) has only a slightly negative influence. On the other hand, parameters Ω and ξ are insignificant and can be excluded from the regression. The weighting factors of the non-negligible parameters (*a*, *b*, *s*, and *d*) for the seven radicals studied are quite similar, indicating that solute−solvent interactions do not depend on the nature of substituents at the α positions. The solute−solvent interactions are therefore governed by the common structural and electronic features of the compounds, i.e., by the interactions that the ONCNO groups of radicals establish with the solvent molecules. This conclusion is consistent with the fact that the O atoms of these groups are the most basic regions of the radicals, as molecular electrostatic potential maps show.[50] One can also explain the solvent preference for these O atoms by looking at the mesomeric forms depicted in Scheme 2, as was previously done for related aminoxyl radicals.[20] Solvents with higher polarities and larger hydrogen bond donor abilities interact favorably with radicals, stabilizing preferentially the mesomeric forms C and D, through the negative charges on the O atoms, increasing the spin density on the N nuclei.

The inspection of independent terms $|a(\mathrm{N})|_0$ of multivariable regressions (Table 3) reveals small but significant differences for each radical. Since these extrapolated values can be taken as estimates of hyperfine coupling constants for isolated molecules in the gas phase, they must reflect, at least in part, the electronic characteristics of the substituents. Thus, the absence of a group at the α position capable of allowing an electronic delocalization, as in radical **1**, produces a significant difference in the spin density distribution of the five-membered ring with respect to α-substituted radicals. Also, an electron-withdrawing substituent at the para position of the phenyl ring (NO_2 group of radical **9**) decreases $|a(\mathrm{N})|_0$ slightly, while electron-donating substituents at the ortho and para positions (OH groups of radicals **4** and **10**) barely increase $|a(\mathrm{N})|_0$ with respect to the nonsubstituted radical **8**. On the other hand, an electron-donating substituent at the meta position (OH group of radical **6**) does not produce any significant difference with respect the value of $|a(\mathrm{N})|_0$ for radical **8**. Finally, two substituents at the ortho and para positions with opposite electronic characteristics (groups Cl and OH of radical **12**) seem to balance their effects.

We now turn our attention into the results of the LSER analyses for the aromatic $|a(\mathrm{H})|$ values of radicals **1**, **4**, **6**, **8**, **9**, **10**, and **12** (Table 3). Regressions for the $|a(\mathrm{H})|$ values corresponding to meta and CH_3 hydrogens were very poor and indicate no solvent dependence. The mean values for the hfcc's are $|a(\mathrm{H_{meta}})| = 0.187(10)$ G and $|a(\mathrm{H_{CH_3}})| = 0.213(10)$ G. In contrast, the $|a(\mathrm{H})|$ values for H atoms at ortho and para positions, as well as for the H atom at the α position of radical

(48) Hildebrand, J. H.; Scott, R. L. *The Solubility of Non-Electrolytes*; Dover Publications: NewYork, 1964.

(49) Taft, R. W.; Gal, J.-L.; Geribaldi, S.; Maria, P.-C. *J. Am. Chem. Soc.* **1986**, *108*, 861−863.

(50) Deumal, M.; Cirujeda, J.; Veciana, J.; Kinoshita, M.; Hosokoshi, Y.; Novoa, J. J. *Chem. Phys. Lett.* **1996**, *265*, 190−199.

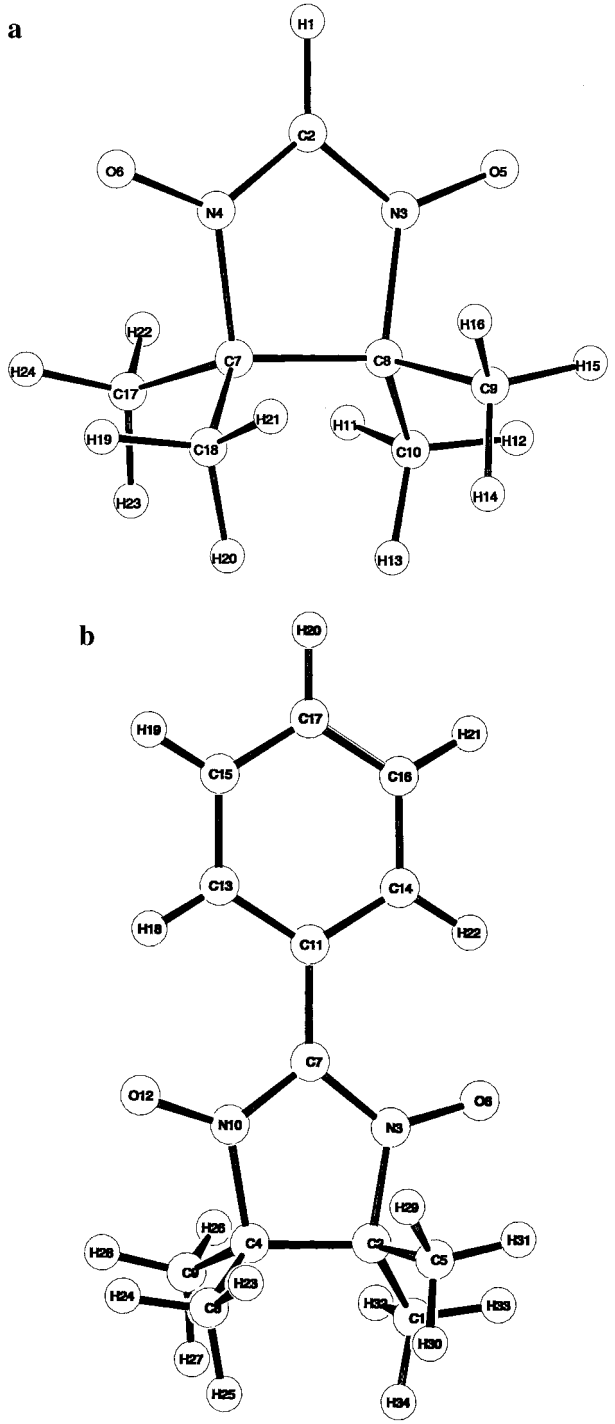

Figure 4. Atomic numbering schemes and optimized geometries obtained for radicals **1** (a) and **8** (b).

1, gave acceptable multivariable regressions, although the quality of regressions was always lower than that obtained for $|a(\mathrm{N})|$ values (probably due to the larger errors present in their determinations). The solvent parameters that proved to be significant for all these regressions were again α, π^*, and δ. The resulting solvent dependence trend for all $|a(\mathrm{H})|$ was the opposite of that for $|a(\mathrm{N})|$. Thus, $|a(\mathrm{H})|$ values decrease with an increase of the solvent polarity and with its hydrogen bond donor ability.

The comparison of $|a(\mathrm{H_{arom}})|_0$ values for radicals with similar steric constraints between the imidazole and phenyl rings validates that the spin density distributions on the phenyl rings

Table 5. Calculated B3LYP/EPR-II Isotropic Hyperfine Coupling Constants (in Gauss) for Optimized ($\varphi = 3°$) and Experimental ($\varphi = 25°$) Geometries of Radical **8** and for Experimental Geometry of Radical **9**

	radical **8**		radical **9**		radical **8**		radical **9**
atom	optim	exptl	exptl	atom	optim	exptl	exptl
C1	+1.29	+0.52	+1.13	H18	+1.22	+1.60	+1.07
C2	−2.48	−2.47	−2.58	H19	−0.49	−0.91	−0.61
N3	+5.60	+6.02	+5.08	X20[a]	+1.11	+1.33	+0.18
C4	−2.48	−2.33	−2.58	H21	−0.49	−0.94	−0.61
C5	+3.65	+3.91	+3.81	H22	+1.22	+1.59	+1.07
O6	−9.49	−10.10	−9.95	H23	−0.21	−0.16	−0.26
C7	−14.98	−16.49	−17.43	H24	−0.30	−0.44	−0.27
C8	+1.28	+0.59	+1.13	H25	−0.30	−0.30	−0.09
C9	+3.65	+3.56	+3.81	H26	−0.41	−0.57	−0.33
N10	+5.59	+5.15	+5.08	H27	+0.52	+0.44	+0.49
C11	+3.83	+4.88	+4.69	H28	−0.70	−0.48	−0.70
O12	−9.48	−9.27	−9.95	H29	−0.41	−0.51	−0.33
C13	−1.88	−2.95	−3.29	H30	+0.52	+0.39	+0.49
C14	−1.88	−3.04	−3.29	H31	−0.70	−0.51	−0.70
C15	+1.41	+1.95	+1.02	H32	−0.21	−0.21	−0.09
C16	+1.41	+2.06	+1.02	H33	−0.30	−0.46	−0.27
C17	−1.58	−2.06	−1.58	H34	−0.30	−0.26	−0.26
				O35			+0.07
				O36			+0.07

[a] X20 is H20 or N20 for radicals **8** and **9**, respectively.

of these radicals are very similar, and, therefore, they are not strongly dependent on the nature and position of substituents on the aromatic rings. In contrast, the previous results also demonstrate the significant effects that surrounding media and solvents have on the hfcc's for α-nitronyl aminoxyl radicals and, therefore, on their spin density distributions. Consequently, it is necessary to use the extrapolated solvent-independent $|a(\mathrm{X})|_0$ values of radicals to compare the ESR hfcc values against those obtained from theoretical calculations.

Theoretical Calculation of hfcc's in α-Nitronyl Aminoxyl Radicals. When the hfcc values for H1, C2, N3, and N4 nuclei of radical **1**,[51] calculated using the B3LYP functional and the EPR-II, cc-pCVDZ, cc-pCVTZ, cc-pVDZ, cc-uspVDZ, cc-pVTZ, and cc-uspVTZ basis sets (Table 4), are compared with the solvent-independent experimental values (Table 3), one finds that the EPR-II, cc-pCVTZ, cc-uspVDZ, and cc-uspVTZ basis sets give results similar in quality. Thus, the calculated hfcc's differ by 2.5−3.5 G with respect to the solvent-independent experimental values. All basis sets also yield a good estimate of the order of magnitude for the average $|a(\mathrm{H})|$ value for the H of the CH_3 groups. Unfortunately, no experimental values are known for the O atoms, but it is interesting to note again the similarity between the EPR-II, cc-pCVTZ, cc-uspVDZ, and cc-uspVTZ basis sets' results. Consequently, given the similar quality between the hfcc's calculated with the EPR-II basis set and those from other, larger basis sets, we decided to use the EPR-II basis set in the rest of our computations. The geometries of the radicals used in these computations were the experimental ones, found in single crystals, except for radicals **10** and **11**, which were optimized, as no single crystals suitable for X-ray diffraction have been grown. The geometrical optimizations were all carried out at the B3LYP/cc-pVDZ level.

In light of the previous results on radical **1**, we decided to evaluate the hfcc's for radical **8**, using the B3LYP functional and the EPR-II basis set. We started by fully optimizing the molecular geometry of this radical without imposing any

(51) The B3LYP/aug-cc-pVDZ-optimized geometry and the experimental geometry for the two known crystalline phases of radical **1** are very similar. The most remarkable deviation observed is for the $C(sp^2)-H$ distance (computed, 1.085 Å; experimental, 0.995 Å in the α phase and 0.921 Å in the β phase).

Table 6. Calculated B3LYP/EPR-II Isotropic Hyperfine Coupling Constants (in Gauss) for the Experimental Geometry of Radicals **4**, **6**, and **10**

	a(X)				*a*(X)		
atom	**4**	**6**	**10**	atom[a]	**4**	**6**	**10**
C1	2.86	1.26	3.03	H18	1.07	1.72	0.51
C2	−2.74	−2.96	−1.29	H19	−0.71	−0.95	−0.24
N3	5.90	5.11	5.18	X20	0.44(O)	1.50(H)	0.43(H)
C4	−2.19	−3.27	−2.99	X21	−0.65(H)	−0.34(O)	−0.20(H)
C5	0.96	3.89	1.02	X22	1.18(H)	−1.61(H)	−0.10(O)
O6	−10.41	−9.73	−6.58	H23	0.06	−0.51	0.80
C7	−15.27	−17.07	−12.60	H24	−0.75	0.32	−0.71
C8	2.34	4.95	4.61	H25	−0.35	−0.70	−0.40
C9	0.67	1.17	1.15	H26	−0.30	−0.21	−0.34
N10	4.91	5.22	5.24	H27	−0.20	−0.25	−0.18
C11	4.62	5.62	2.78	H28	−0.25	−0.48	−0.31
O12	−8.86	−10.18	−11.07	H29	−0.33	−0.36	−0.09
C13	−2.52	−2.92	−1.42	H30	−0.27	−0.22	−0.16
C14	−2.57	−2.71	−1.96	H31	−0.26	−0.30	−0.21
C15	1.48	2.19	0.46	H32	−0.73	−0.05	0.65
C16	1.36	2.55	0.35	H33	−0.28	−0.39	−0.59
C17	−1.65	−2.17	−0.51	H34	0.25	−0.26	−0.43
				H35	0.32	−0.09	−1.07

[a] Atoms X20, X21, and X22 are the H or O atoms attached to the ortho, meta, and para positions, and H35 is the hydrogen of the hydroxyl group.

symmetry restriction. The B3LYP/cc-pVDZ optimum geometry (Figure 4; see also Table S1 in Supporting Information) is in excellent agreement with the experimental X-ray data, with the exception of the torsion angle (φ) between phenyl and imidazole rings. The calculated φ angle is close to 0°, while the experimental one is 25°.[4c] Given this striking difference, we tested whether this result was a feature of the B3LYP method by reoptimizing the geometry at the UHF, MCSCF(3,3), and MP2 levels. The optimum angles with these three methods were also close to 0°. The same torsion angle was found after geometrical optimizations in radicals **4**, **6**, **8**, **9**, and **10.** Therefore, we have to attribute the nonzero torsion angle found in the crystals of this family of radicals to intermolecular interactions (crystal packing forces) that the six-membered ring undergo in the crystals[42] and the small energy increment involved for low rotation angles.

The hfcc's calculated for radical **8** at the B3LYP/EPR-II level are collected in Table 5 for the experimental and optimized geometries (the same property was also computed using the cc-pVDZ and cc-us-pVDZ basis sets, and the resulting data are gathered in as Supporting Information, Table S2). Comparing the hfcc's calculated at the B3LYP/EPR-II level for both conformations, it becomes clear that the torsion angle φ has only a small effect on the hfcc values: (a) the sign and order of magnitudes are preserved in both conformations, (b) the mean of absolute values for the differences of hfcc's is 0.78 G, and (c) the largest deviation observed for the hfcc's of both conformations is 1.5 G for the C7 atom. As expected, the loss of planarity between the five- and six-membered rings decreases the ring conjugation and induces a loss of spin delocalization, and the hfcc's of the phenyl H atoms decrease. In addition, there is an acceptable agreement of the two sets of values with the experimental hfcc's of Table 3 for the N nuclei, but the computations give a larger negative value for the C7 atom. The relative magnitudes of hfcc's for the atoms in the five- and six-membered rings are also predicted properly. Thus, the hyperfine coupling of the ortho-H nuclei (H18, H22) are larger than for the para one (H20), and the latter is larger than those for the meta nuclei (H19, H21). In addition, the alternating signs of these hfcc's are in good agreement with the experimental evidence obtained from ^{1}H NMR studies.[4h,12,15] As was already found for radical **1**, the calculations reproduce also the small averaged nuclear spin density on the H atoms of methyl groups (H23−H34) observed by ESR.

We decided then to focus our attention on the computed hfcc's of radical **9** at the B3LYP/EPR-II (Table 5) and B3LYP/cc-pVDZ (Table S3) levels using the experimental crystal geometry. Results similar to those described for radical **8** were found in this radical when the values were compared with the extrapolated solvent-independent values. To facilitate the comparison of the computed hfcc's of radical **9** with those of radical **8**, we have used the same atom numbering scheme in both radicals. Thus, the N of the nitro group occupying the position of the H20 atom in radical **8** is the N20, with the O35 and O36 atoms being the two O atoms of the nitro group. A comparison of the hfcc's (Table 5) shows that the inclusion of the nitro group in radical **8** induces very small changes in the hfcc's: (a) the sign and order of magnitude are preserved in all atoms, (b) the mean of absolute values for the differences between hfcc's

Table 7. Calculated B3LYP/EPR-II Isotropic Hyperfine Coupling Constants (in Gauss) for the Experimental Geometry of Radicals **5**, **7**, **11**, and **12**

	a(X)					*a*(X)			
atom	**5**	**7**	**11**	**12**	atom[a]	**5**	**7**	**11**	**12**
C1	4.05	1.10	2.92	1.10	H18	1.80	1.31	0.90	0.92
C2	−2.47	−2.17	−1.37	−2.67	X19	−0.31(O)	−0.26(O)	−0.54(H)	−0.69(H)
N3	5.41	4.98	5.23	5.25	X20	1.63(H)	0.55(O)	0.44(O)	0.29(O)
C4	−1.84	−2.92	−2.85	−2.22	X21	−0.29(O)	−0.87(H)	−0.51(H)	−0.57(H)
C5	0.78	3.83	0.90	3.57	X22	1.72(H)	1.71(H)	0.05(O)	−0.10(Cl)
O6	−10.72	−9.53	−7.32	−10.12	H23	−0.71	−0.71	−0.34	−0.36
C7	−17.27	−16.95	−14.36	−17.65	H24	0.49	0.64	0.51	−0.66
C8	0.80	1.53	1.06	3.40	H25	−0.36	−0.34	−0.68	0.50
C9	3.82	4.98	4.24	1.30	H26	−0.23	−0.30	−0.25	−0.31
N10	4.91	5.66	5.45	5.69	H27	−0.23	−0.29	−0.30	−0.21
C11	6.33	5.36	3.87	4.97	H28	−0.23	−0.20	−0.29	−0.22
O12	−9.98	−10.35	−11.27	−9.89	H29	−0.25	−0.26	−0.24	−0.19
C13	−3.06	−2.94	−2.08	−3.48	H30	−0.28	−0.23	−0.15	−0.30
C14	−3.10	−3.17	−2.74	−4.32	H31	−0.20	−0.25	−0.20	−0.30
C15	2.66	1.79	1.11	0.92	H32	−0.36	−0.60	0.51	−0.33
C16	2.62	2.03	1.03	1.10	H33	−0.73	0.15	−0.45	−0.63
C17	−2.24	−2.01	−1.32	−1.25	H34	0.75	−0.35	−0.59	0.64
					H35	−0.07	−0.08	−0.66	0.16
					H36	−0.07	0.30	−1.25	n.e.

[a] Atoms X19, X20, and X21 are the H or O atoms attached to the ortho, meta and para positions, and H34 and H35 are the hydrogen of hydroxyl groups. Cl atom in radical **12** is X22.

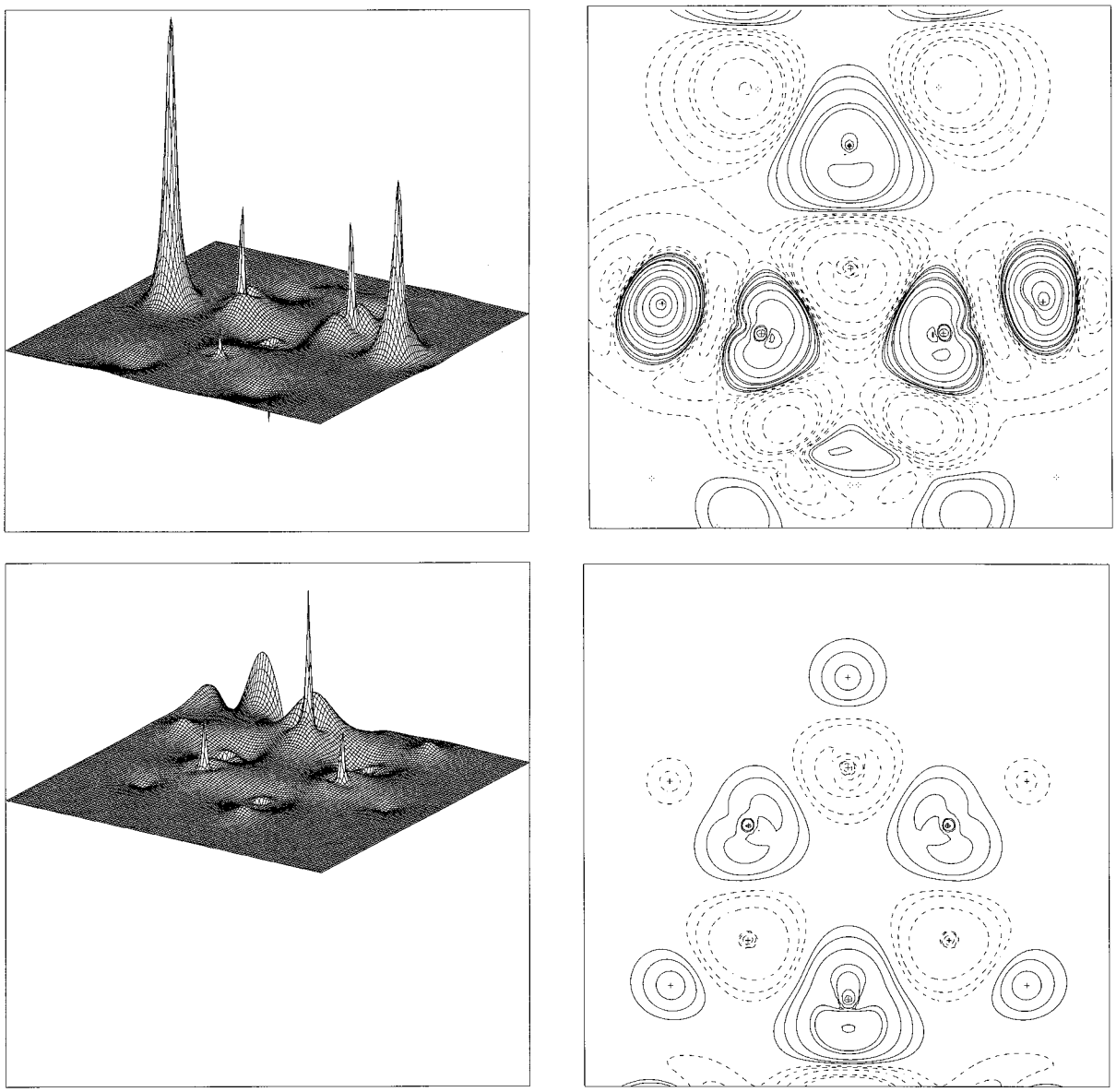

Figure 5. Spin density map for the experimental crystal geometry of radical **8**, computed at the B3LYP/cc-pVDZ level, in the form of contour map (left) and contour lines (right; continuous and discontinuous lines indicate positive and negative spin densities, respectively) for the five- (top) and six-membered rings (bottom) of the molecule. The scale of the map corresponding to the aromatic part is enlarged 10 times in order to show all details.

is 0.42 G, and (c) the largest deviation is 0.9 G and occurs at the C7 atom. It is also interesting to note that the NO_2 hfcc's are similar to the values found for the aromatic H atoms.

We have also computed at the B3LYP/EPR-II level the hfcc's of the monosubstituted radicals **4**, **6**, and **10** (Table 6) and the disubstituted radicals **5**, **7**, **11**, and **12** (Table 7). The values obtained for all these radicals reproduce the trends found for extrapolated solvent-independent values. Moreover, they also indicate that the degree of substitution of the six-membered benzene ring does not have an important effect on the spin density distribution of radicals.

Theoretical Spin Density Maps in Isolated Radicals. The experimental values of the hfcc's are excellent proofs for the spin density on the nuclei and, therefore, can help us to get a first estimate of the electronic spin distribution over the molecule. However, as they depend only on the spin density on the nuclei, they can give misleading impressions of the size of the atomic spin population on a given atom, which is the sum of the spin density over the three-dimensional space assigned to that atom. For non-H atoms, the *n*p and *n*d orbitals have null values on the nucleus but have maxima far away from it, and the same is true for the *n*s (with $n > 1$) atomic orbitals. Consequently, the spin density on the nucleus is not always a good representation of the spin localized on that atomic region. Therefore, if we want to get a complete picture of the distribution of the spin density on the whole molecular space, we have to use experimental techniques that probe the whole space, as in the case of the PND technique. The information on the spin density distribution obtained in these studies is presented in the form of spin density maps, which present the value of the spin density at any point of space around the molecule. They are computed by subtracting the electronic density of the α and β electrons. Consequently, the spin can be positive or negative, indicating in the first case regions where more α spins are located. The spin density maps also give direct information on the presence of spin on atoms that, in principle, do not present unpaired electrons. From these spin maps, it is possible to define the amount of spin associated with each atom if we properly

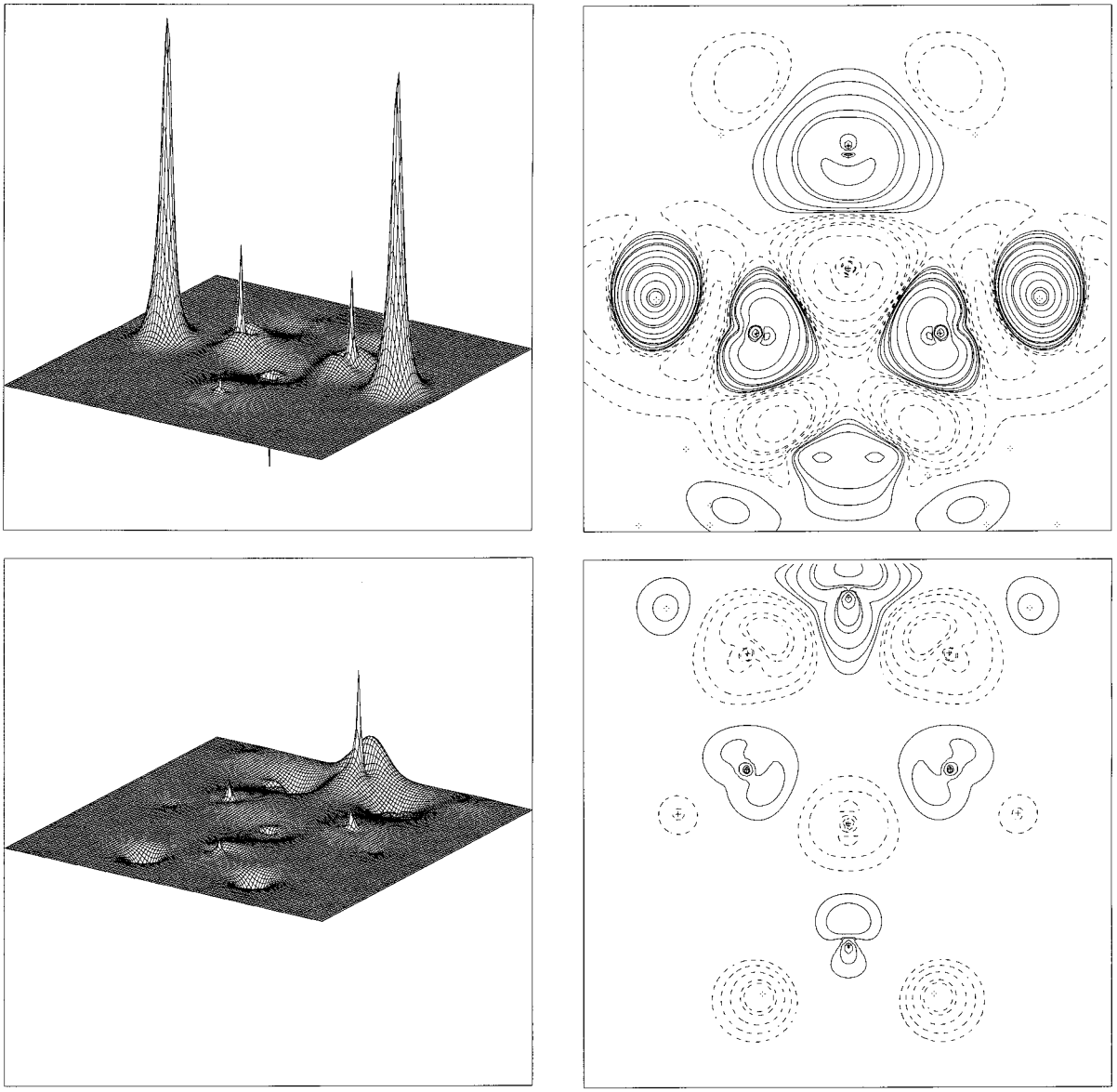

Figure 6. Spin density map for the experimental crystal geometry of radical **9**, computed at the B3LYP/cc-pVDZ level, in the form of contour map (left) and contour lines (right; continuous and discontinuous lines indicate positive and negative spin densities, respectively) for the five- (top) and six-membered rings (bottom) of the molecule. The scale of the map corresponding to the aromatic part is enlarged 10 times in order to show all details.

define the regions of space which correspond to each atom by means of a projection technique. In such a way we can talk about atomic spin populations, which are simplified forms of the information contained in the spin density maps.

Defining the space of the molecule that corresponds to a given atom is not an easy task and can only be done in a rigorous quantum mechanical form within the atoms-in-molecules (AIM) theoretical framework.[52] In the AIM theory, the space of the molecule assigned to each atom is defined as the part of the three-dimensional space around the nucleus (attractor) enclosed within regions of zero flux of the electronic density gradient.[52] Then, the atomic spin population is computed as the integral of the molecular spin density within this region. The computation of AIM atomic spin population is very costly. Therefore, one normally resorts to simplified and approximate procedures, such as the Mulliken population analysis.[53] Such a method is fast, but its results are not independent from the unitary transformations of the molecular orbitals. Besides, if the basis set is not well balanced, it can show artifact charge transfers among neighboring atoms. Nevertheless, we have already show in previous works that the atomic spin population for radical **1** obtained using the Mulliken population analysis method is very close to the AIM population.[17b] The same conclusion was proven to be valid here for radical **8**.

We can now evaluate the similarity between the spin distribution maps computed at the B3LYP/EPR-II (and B3LYP/cc-pVDZ) level for radicals **8** and **9** at their experimental nonplanar geometries. Figures 5 and 6 show the EPR-II spin density maps for both radicals, which are indistinguishable from the cc-pVDZ ones. These maps are represented as two separate contour maps: one represents the spin density in the mean plane of the five-membered ring and the other the density on the mean plane of the six-membered ring. We chose this option instead of plotting the surface of a constant spin value,[17b] because in

(52) Bader, R. F. W. *Atoms in Molecules, A Quantum Theory*; Clarendon Press: Oxford, 1990.

(53) Szabo, A.; Ostlund, N. S. *Modern Quantum Chemistry*; Macmillan: New York, 1982; p 151.

Table 8. Calculated B3LYP/EPR-II Mulliken Atomic Spin Populations (in e) for the Experimental Geometries of Radicals **8** and **9**

atom	**8**	**9**	atom	**8**	**9**
C1	+0.001	+0.001	H18	+0.003	+0.002
C2	−0.010	−0.012	H19	−0.002	−0.001
N3	+0.291	+0.273	X20[a]	+0.003	+0.002
C4	−0.013	−0.012	H21	−0.002	−0.001
C5	+0.018	+0.018	H22	+0.003	+0.002
O6	+0.350	+0.348	H23	0.000	0.000
C7	−0.215	−0.235	H24	−0.001	0.000
C8	+0.001	+0.001	H25	0.000	0.000
C9	+0.021	+0.018	H26	−0.001	0.000
N10	+0.263	+0.273	H27	+0.001	+0.001
C11	+0.050	+0.030	H28	−0.001	−0.001
O12	+0.324	+0.348	H29	−0.001	−0.000
C13	−0.048	−0.028	H30	+0.001	+0.001
C14	−0.047	−0.028	H31	−0.001	−0.001
C15	+0.028	+0.018	H32	0.000	0.000
C16	+0.030	+0.018	H33	−0.001	0.000
C17	−0.043	−0.025	H34	−0.001	0.000
			O35		−0.003
			O36		−0.003

[a] X20 is H20 or N20 for radicals **8** and **9**, respectively.

the later case the internal structure of the spin distribution is lost, and first contour maps are directly comparable with those obtained from the PND studies.

Comparison of Figures 5 and 6 shows the close similarity of the spin distribution in both molecules. The two figures present most of the spin density localized on the ONCNO part of the molecule with a positive spin on the N and O atoms and a negative spin on the α C atom. The spin map for radical **8** shows an unexpected asymmetry between the two N−O groups. Nevertheless, a detailed analysis indicated that the asymmetry is caused by the absence of symmetry in the experimental crystal geometry of the five-membered ring (for instance, one of the N−O distances is 0.01 Å shorter than the other, and the same is true with the C(sp^2)−N distances, which differ by 0.03 Å). After fully optimizing the geometry of radical **8**, we obtained a symmetrical conformation for the five-membered ring, which does not present any important difference in the distances of the two NO groups. For this optimum geometry, the corresponding spin map (see Figures S1−S4 in the Supporting Information) shows a symmetrical spin distribution on the two NO groups.

The similarity of the spin density distributions of radicals **8** and **9** is also reflected in the atomic spin populations, computed at the B3LYP/EPR-II level, on the equivalent atoms, as shown in Table 8 (see also Table S4 for data computed at the B3LYP/cc-pVDZ level). Such atomic spin populations indicate a preference for the O atoms with respect the N atoms, 50% larger in the O atom than in the N atom, which was also found in DFT calculations for radical **8**.[4d] This feature contrasts with the similar spin populations found experimentally on O and N atoms with the PND technique.[4] Another result of B3LYP/EPR-II computations worth noticing is the large negative spin population found for the α C atoms of radicals **8** and **9**. This result contrasts with the less negative value obtained by DFT for radical **8**, which is closer to that found experimentally with PND.[4] Another interesting point is the spin population on the atoms of the six-membered ring. Thus, the spin population on the aromatic C atoms is around 10 times smaller than on the ONCNO atoms and is evenly distributed with sign alternation between consecutive atoms. Moreover, the spin population on the H atoms attached to the aromatic C atoms is even smaller, and the atoms are more localized. Thus, the atomic spin population in these H atoms is always less than 0.002 e. Similar small atomic spin population is also found in the H atoms of the methyl groups.

The similarity of spin density maps of radicals **8** and **9** indicates that the nitro group has a very small influence on the spin density distribution. Computations on the monohydroxilated radicals **4**, **6**, and **10** reflect the same trend on the small influence of OH groups. This opens the following question: Why do these groups not affect the spin distribution on these substituted phenyls? We can rationalize this fact in terms of a qualitative molecular orbital fragment analysis. In essence, the spin-donating atoms are the two NO groups (each presenting one unpaired spin) and the α C atom (another unpaired spin). The most stable combination of these three spin-donating centers is a doublet that delocalizes the charge over the ONCNO group. As ab initio computations on radical **1** show, the SOMO orbital is a nonbonding orbital having a node in the α C atom and opposite sign in each NO group. Therefore, an ROHF or extended Hückel computation cannot describe the negative spin on the α C atom. This can only be described by using methods that use more than one ROHF determinant. The spin delocalization is a consequence of the presence of more than one ROHF wave function in the exact multiconfigurational wave function. Thus, a simple MCSCF(2,2) computation properly describes the spin delocalization in radical **1**, although a good description of all the physics of this problem is obtained with a MCSCF(3,3) computation. An UHF wave function is capable of describing that spin delocalization because, as was recognized long time ago,[54] it gives the same results as a limited CI computation. Unfortunately, the strong spin contamination that the UHF wave function presents makes the results obtained from this method useless. The presence of spin in the six-membered ring can only come from the spin delocalization mechanism; that is, excitations from the ground ROHF determinant to some excited one in which the excited determinant present orbitals with a large contribution from the six-membered ring atoms. Our computations indicate that the orbitals of the five-membered ring are much lower in energy than those in the substituted six-membered ring. Therefore, they do not mix too much. Furthermore, the excitations from the SOMO, localized on the five-membered, to the six-membered ring orbitals are very energetic. Consequently, their weight in the multiconfigurational wave function is not very large, thus decreasing the amount of spin delocalization from the five- to the six-membered ring. Therefore, to increase the amount of spin delocalization in these radicals, one should add as many strong electronegative functional groups as possible to the six-membered ring in order to stabilize its fragment orbitals, although this approach is not applicable to the radicals that we have tested here. The presence of many strong electronegative substituents on the six-membered ring should decrease the persistence of radicals, making this approach useless for preparing organic molecular magnets.[55]

We do not want to finish our evaluation of the B3LYP spin density maps of α-nitronyl aminoxyl radicals without emphasizing that the B3LYP results reproduce the main features experimentally observed using the PND technique for the five-membered ring. The discrepancies found in the six-membered ring seem to indicate precision problems in the PND fitting, as one should always expect sign alternation in these maps. Thus, the B3LYP maps could be used to study the low-density regions that are difficult to describe with precision in the PND technique.

(54) (a) Pulay, P.; Hamilton, T. *J. Chem. Phys.* **1988**, *88*, 4926. (b) Bofill, J. M.; Pulay, P. *J. Chem. Phys.* **1989**, *90*, 3637.

(55) Unpublished results; see: Cirujeda, J. Ph.D. Thesis, Universitat Ramón Llull, Barcelona, 1997.

Concluding Remarks

The results obtained with the hfcc's of the studied series of substituted α-nitronyl aminoxyl radicals demonstrate that the spin density distribution on the phenyl ring is not strongly dependent on the nature and positions of substituents on the aromatic ring. In contrast, the hfcc's show a significant solvent dependence. The study by the LSER method has allowed us to demonstrate that the most influential properties of the solvent are the polarity/polarizability and its ability to donate/accept hydrogen bonds. The estimates of solvent-independent hfcc's for α-nitronyl aminoxyl radicals can be used directly to test the level of accuracy of any theoretical computation of the spin density distribution of this family of radicals. Thus, although some discrepancies have been found between the experimental and theoretical values, calculated at the B3LYP/EPR-II level (for instance, for the C7 atom of radicals **8** or **9**), the ab initio calculations reproduce the trends of hfcc's found experimentally as well as the atomic spin populations obtained by PND. Overall, the quality of the B3LYP calculations is enough to reproduce the main features of atomic spin density distributions and to explain experimental trends observed in α-nitronyl aminoxyl radicals, even in regions of vanishingly small spin densities.

Acknowledgment. This work was supported by grants from DGES (PB96-0862-C02-01 and PB95-0848-C02-02), CIRIT (1998SGR-96-00106), and the 3MD Network of the TMR program of the E.U. (Contract ERBFMRX CT980181). The allocation of CPU time in the CESCA-CEPBA computers was made possible by the CIRIT-University of Barcelona program, which is also acknowledged. The authors thank to D. B. Amabilino (ICMAB, CSIC) for correcting the manuscript and his useful comments, and also F. Köhler (Technische Universität München, Germany) for his valuable suggestions to this work. J.C. and O.J. also thank the Generalitat de Catalunya for their fellowships.

Supporting Information Available: Optimized geometry (Table S1), calculated isotropic hyperfine coupling constants (Table S2), and spin density map (Figures S1S4) computed at the B3LYP/cc-pVDZ level for the optimized geometry of radical **8**; calculated isotropic hyperfine coupling constants computed at the B3LYP/cc-pVDZ level for the optimized geometry of radical **9** (Table S3); calculated B3LYP/cc-pVDZ Mulliken atomic spin population for experimental geometries of radicals **8** and **9** (Table S4) (PDF). This material is available free of charge via the Internet at http://pubs.acs.org.

JA0004884